Multispectral fluorescence imaging: Zhou and El-Deiry provide an overview of this rapidly growing field, focusing on applications in small animal imaging and in flow cytometry and on the clinical potential across a range of diagnoses and therapies. . . . . ***Page 1563***

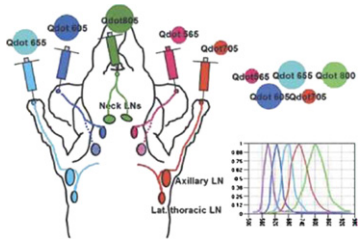

Imaging tumor phenotype: Mankoff and Dehdashti review the importance of tumor phenotype characterization for personalized cancer treatment and preview an article in this issue of *JNM* on combined molecular imaging studies to assess estrogen receptor expression. . . . . ***Page 1567***

Weight-based pediatric PET/CT: Alessio and colleagues describe PET/CT acquisition protocols customized to children's weight and estimate the dosimetry and cancer risk associated with these low-dose procedures. . . . . ***Page 1570***

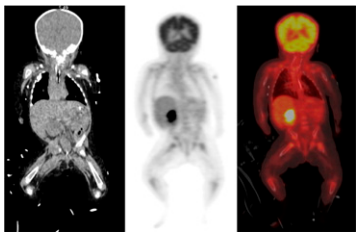

Breath-hold PET/CT in lung cancer: Torizuka and colleagues compare tumor ^{18}F-FDG uptake in a single 20-s acquisition of deep-inspiration breath-hold PET/CT with that in free-breathing PET/CT in patients with lung cancer. . . . ***Page 1579***

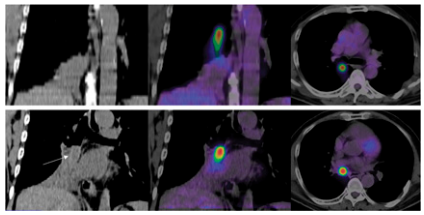

^{11}C-choline PET/CT in prostate cancer: Piert and colleagues use multimodality fusion techniques, including MRI and histology data, to assess whether ^{11}C-choline PET/CT can serve as a marker of tumor aggressiveness in primary adenocarcinoma of the prostate. . . . . ***Page 1585***

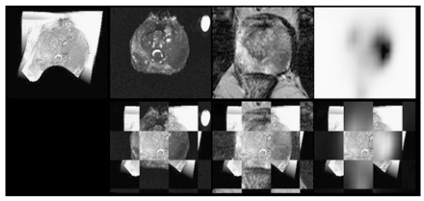

Observer variation in lymphoma staging: Hofman and colleagues quantify levels of observer agreement in interpretation of PET/CT staging images in patients with lymphoma. . . . . ***Page 1594***

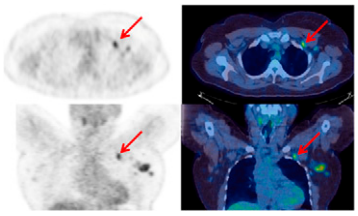

PET index for endometrial cancer: Tsujikawa and colleagues investigate whether ^{18}F-FES and ^{18}F-FDG PET data can be combined to accurately predict tumor aggressiveness in patients with endometrial cancer. . . . . ***Page 1598***

RAI and salivary gland side effects: Grewal and colleagues detail the incidence, time course, dose-response factors, and ultimate resolution of salivary gland complications in patients receiving radioactive iodine for remnant ablation or therapy in thyroid cancer. . . . . ***Page 1605***

PET/CT and vascular risk prediction: Rominger and colleagues evaluate the association of arterial ^{18}F-FDG uptake and calcifications in large arteries as detected by ^{18}F-FDG PET/CT with subsequent occurrence of vascular events in otherwise asymptomatic cancer patients. . . . . ***Page 1611***

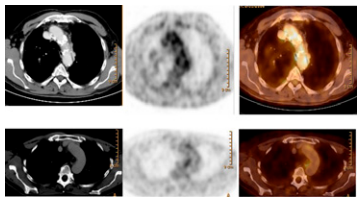

Coronary CTA and SPECT fusion: Slomka and colleagues describe an automated technique for myocardial SPECT and 64-slice CT angiography registration with resulting improved quantification using coregistered physiologic and anatomic data. . . . . ***Page 1621***

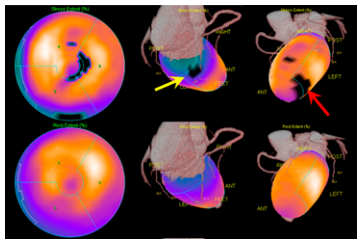

NP-59 SPECT/CT in adrenal adenoma: Yen and colleagues explore the diagnostic utility of ^{131}I-NP-59 adrenal SPECT/CT in differentiating aldosterone-producing adenoma from idiopathic adrenal hyperplasia and in predicting postoperative outcomes in patients with inconclusive diagnoses on venous sampling and CT alone. . . . ***Page 1631***

^{18}F-FDG and ^{123}I-β-CIT dementia imaging: Lim and colleagues report on techniques to optimize interpretation of ^{18}F-FDG PET images for differentiating dementia with Lewy bodies from Alzheimer disease and compare the results with dopamine transporter imaging using ^{123}I-β-CIT SPECT. . . . . ***Page 1638***

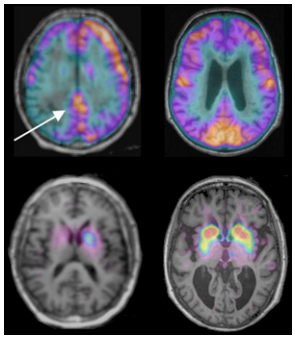

^{18}F-FDG PET repeatability in multicenter trials: Velasquez and colleagues assess the repeatability of several semiquantitative standardized uptake values on baseline ^{18}F-FDG PET studies with centralized quality assurance in a multicenter phase I oncology trial. . . . . ***Page 1646***

PET/CT for RT: Ford and colleagues provide an educational overview of the benefits and challenges of ^{18}F-FDG PET/CT in radiation therapy planning and describe novel radiopharmaceuticals under investigation for PET imaging in this setting. . . . . ***Page 1655***

PEM Flex Solo II performance: MacDonald and colleagues report on performance characteristics of this commercial positron emission mammography camera and, in the absence of specific standards for assessing such systems, propose tests that should be included in standardized testing. . . . . ***Page 1666***

Optical imaging of granuloma formation: Eisenblätter and colleagues determine whether fluorescence reflectance imaging and fluorescence-mediated tomography allow for the visualization and quantification of early inflammatory processes in vivo. . . . . ***Page 1676***

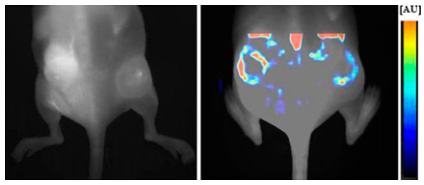

^{99m}Tc-Anti-CD3 for T-cell imaging: Malviya and colleagues describe studies with a radiolabeled anti-CD3 antibody for high-resolution γ-camera imaging of T-cell traffic and lymphocytic infiltration of tissues and organs affected by autoimmune diseases. . . . . ***Page 1683***

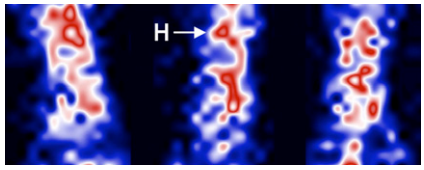

^{18}F-FBZA for melanoma metastasis imaging: Ren and colleagues explore the utility of radiolabeling a benzamide with an affinity for melanin and describe its ability to identify melanotic metastases in preclinical studies. . . . . ***Page 1692***

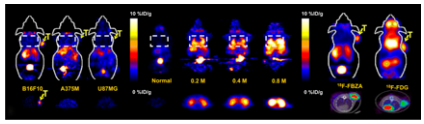

^{213}Bi RIT in bladder cancer: Pfost and colleagues report on an orthotopic human bladder carcinoma mouse model and on the comparative immunotherapeutic efficacies of intravesically instilled ^{213}Bi-anti-epidermal growth factor receptor monoclonal antibody and mitomycin C. . . . . ***Page 1700***

^{18}F-FPA PET in prostate cancer: Pillarsetty and colleagues describe the synthesis of and small-animal PET studies with this novel tracer with potential for diagnosis and therapy monitoring in prostate cancer. . . . . ***Page 1709***

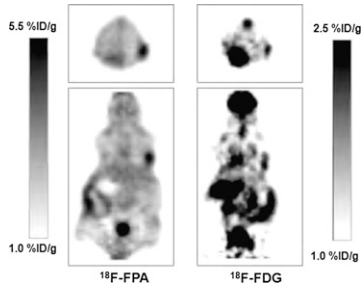

Biomathematic radioligand screening: Guo and colleagues introduce a biomathematic modeling approach that aims to predict the in vivo performance of radioligands directly from in silico/in vitro data, assisting in the development of PET and SPECT molecular imaging probes. . . . . ***Page 1715***

Radiosynthesis of 6-^{18}F-fluoro-L-DOPA: Wagner and colleagues detail a novel 3-step, "1-pot" isotopic exchange process for the preparation of this widely used radiopharmaceutical. . . . . ***Page 1724***

Performance of microPET Focus 120: Bahri and colleagues evaluate the image quality and accuracy of attenuation and scatter corrections provided with the microPET Focus 120 scanner using a National Electrical Manufacturers Association image quality phantom. . . . . ***Page 1730***

ON THE COVER

^{18}F-FDG PET/CT is being used in a variety of diseases to better delineate target tumor boundaries before radiotherapy. Here, for a patient with pancreatic cancer, the yellow outline based on the CT scan was made by a radiation oncologist, whereas the blue outline based on the PET scan was made by a nuclear medicine physician. The difference between the 2 outlines reflects a real difference between apparent tumor locations on the 2 studies.

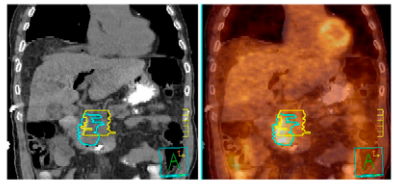

See page 1656.